Journal of Imaging Science and Technology® 54(4): 040501–040501-14, 2010.

Anisotropic Three-Dimensional Wavelet-Based Method for Multi/Hyperspectral Image Compression and Its Benchmark

Jonathan Delcourt, Alamin Mansouri, Tadeusz Sliwa and Yvon Voisin
University of Burgundy, Laboratoire Le2i, BP 16 Route des Plaines de l'Yonne, 89010 Auxerre Cedex, France
E-mail: alamin.mansouri@u-bourgogne.fr

Abstract. *In this article, the authors investigate multi/hyperspectral image compression strategies when data and conditions change. In particular the authors compare the classical multi-two-dimensional (2D wavelets and 2D SPIHT) and hybrid (3D wavelets and 2D SPIHT) strategies to full 3D, for which the authors propose a new implementation based on anisotropic 3D wavelets followed by a 3D SPIHT encoder. All strategies are combined with a spectral principal component analysis decorrelation stage to optimize performance. The comparison of the proposed strategy with the other is made with regard to variations in bitrate, spatial, and spectral dimensions of the images. For consistent evaluation, the authors also propose a larger evaluation framework than the conventionally used PSNR, including nine metrics divided into four families. The authors also study the effect of compression by tiles and discuss the time and memory consumption difference between the three compression strategies. Good results are obtained for the proposed method and the benchmark shows the weaknesses and strengths of each strategy. © 2010 Society for Imaging Science and Technology.*
[DOI: 10.2352/J.ImagingSci.Technol.2010.54.4.040501]

INTRODUCTION

Multi/hyperspectral images offer several advantages over conventional RGB imaging and have therefore attracted increasing interest in the past few years. Indeed such imaging techniques are increasingly used in geoscience, remote sensing, quality control in industry, meteorology, exact color measurements, etc. The resolution in the spatial and spectral dimension increases as better multi/hyperspectral sensors are developed resulting in a large amount of data. However, limitations in transmission speed and storage capacity require the development of suitable compression methods for multi/hyperspectral images.

A multi/hyperspectral image could be represented as a three-dimensional (3D) cube with one spectral and two spatial dimensions. The fact that a multi/hyperpectral image consists of a series of narrow and contiguously spectral bands of the same scene produces a highly correlated sequence of images. This particularity differentiates multi/hyperspectral images from volumetric ones with three isotropic spatial dimensions and also from videos with one temporal and two spatial dimensions. So, conventional compression methods are not optimal for multi/hyperspectral image compression. Therefore compression algorithms need to be adapted to this type of image and often require a decorrelation stage following spectral dimension.

One of the most efficient compression methods for monochrome image compression is the JPEG2000 (http://www.jpeg.org). Its extension to multi/hyperspectral images yields different strategies. These strategies depend on the manner of which one considers the multi/hyperspectral cube after the decorrelation stage (Figure 1):

- Each image band of the multi/hyperspectral image is considered separately [two-dimensional (2D) wavelets +2D set partitioning in hierarchical trees (SPIHT)]: the multi-2D strategy (M2D).
- The whole cube is considered as input leading to two main implementations: the hybrid strategy (3D wavelets+2D SPIHT) and the full 3D strategy (F3D). For these latter we propose an anisotropic 3D wavelets decomposition (3D wavelets+3D SPIHT).

We implement the three compression strategies with the same lifting scheme wavelet transform and compare them. To provide a more objective benchmark, we propose a

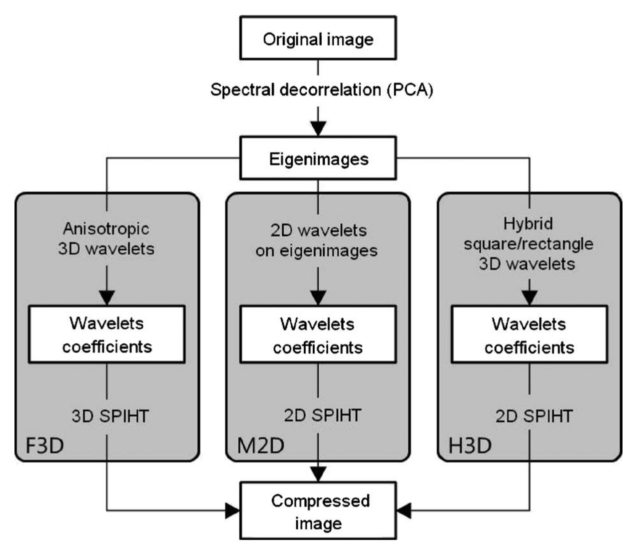

Figure 1. Summary of benchmarked compression strategies.

Received Nov. 1, 2009; accepted for publication Mar. 24, 2010; published online Jun. 15, 2010.
1062-3701/2010/54(4)/040501/14/$20.00.

framework of evaluation composed of eight metrics in addition to the classic PSNR. These metrics evaluate the quality of reconstruction in terms of signal, spectral reflectance, perceptive aspects, and classification driven metrics.

In the next section, we provide a short overview of how we use the principal component analysis (PCA) algorithm within the three compression strategies before describing them. The third section introduces the framework of comparison by splitting the metrics into four categories and gives the explicit formula of each metric. We show experimental results in the fourth section before discussing them in the fifth section. Conclusions are presented in the final section.

We can summarize the contributions of the article in:

- Proposition of an anisotropic-3D-wavelet-based method for the full 3D strategy.
- Proposition of a large evaluation framework (four families of metrics).
- Benchmarking the three strategies by varying bitrates, data, and spatial and spectral dimensions.
- We also use the three different compression strategies with tiling and compare complete compression and compression by tile.
- In order to take the algorithmic aspects of these strategies into account, we will also discuss them in terms of time and memory consumption.

COMPRESSION STRATEGIES

For the implementation of the three strategies we chose to use the wavelets of JPEG2000 standard[1–5] because it is a reference for 2D compression. The JPEG2000 standard wavelets are "Le Gall 5/3" for lossless compression and "Cohen-Daubechies-Feauveau 9/7" (or CDF 9/7) for lossy compression. In our case we perform lossy compression, so we will use the CDF 9/7 wavelet.

Multi/hyperspectral images have a high correlation between image bands. To achieve the best compression ratios it is necessary to take this correlation into account.

PCA Decorrelation

In order to optimize multi/hyperspectral image compression, a decorrelation step is often used. In this context, several methods have been developed. Classic algorithms are based on vector quantization,[6] wavelets, or hybrid methods, such as differential pulse code modulation-discrete cosine transform (DPCM-DCT),[7] Karhunen-Loève transform-discrete cosine transform (KLT-DCT),[8] and PCA (KLT). The PCA has been shown to be one of the most efficient spectral decorrelators[9] and is used in many compression methods.

Epstein et al. propose in Ref. 10 a method for landsat thematic mapper multispectral imagery. The method first removes interband correlation by PCA to produce principle components of seven landsat bands. The principle components are then compressed using wavelet and lossless compression techniques such as run length encoding. Harsanyi and Chang[11] applied PCA to hyperspectral images to reduce data dimensionality, suppress undesired or interfering spectral signatures, and classify the spectral signatures of interest. Mielikäinen and Kaarna[12] applied PCA to reduce correlation among spectral bands, but they only selected a small number of spectra from the image for the calculation of the eigenvectors. They then applied integer wavelet transform to the residual image to concentrate energy and reduce entropy. Du and Fowler implemented PCA along with JPEG2000 for hyperspectral image compression.[13] They assumed that PCA would help in spectral decorrelation and JPEG2000 would help in compression. They found that the method performed better than the combination scheme of wavelet for spectral decorrelation and JPEG2000 for compression. They tested both methods and found that, for rate distortion and information preservation, PCA with JPEG2000 outperformed JPEG2000 alone.

Other spectral decorrelators based on PCA may be used. In Ref. 14, adaptive KLT is use for decorrelation. The original image is divided into proper regions and transforms each region image data set by the corresponding transformation function. The results of their simulations show that the performance of adaptive KLT is better than KLT alone. Gu et al.[15] proposed a kernel based nonlinear subspace projection (KNSP) method followed by kernel PCA. They partitioned the full data space into different subspaces. Next, they used kernel PCA for feature selection based on class separability criteria. The authors claim that the method is more suitable for feature extraction than linear PCA and segmented linear component transformation, particularly when hyperspectral data have nonlinear characteristics.

Some compression algorithms are optimized for specific applications (classification, visualization, dimension reduction, etc.). For this they will use PCA variants. In our case we simply seek to compress without knowledge of the final image utilization, which is why we use classical PCA, which does not favor any particular use.

In our experiments, we applied PCA to the original multi/hyperspectral image in the spectral dimension. As a result, we obtain a new multiband image in the transform domain in which the spectral correlation is reduced. The image bands in the transform domain were sorted with decreasing variance (according to the values of the eigenvalues). We finally applied the three compression strategies to all bands of the transformed image, unlike in dimension reduction[11–13,15] where only a few bands were selected. This procedure allowed us to preserve the maximum amount of image information.

Full 3D strategy

The F3D strategy consists of considering the whole multi/hyperspectral image cube as an input for an 3D wavelet transform. In our case the input is the eigenimages cube resulting from the PCA. Then a 3D extension of SPIHT encoder[16] is applied. The 3D SPIHT encoder of Kim et al.[17] is appropriate to the 3D block shape of the decomposition (Fig. 1). Dragotti et al. also propose a 3D extension of SPIHT but with temporal compensator for video coding;[18] this coder is not appropriate in the case of multi/hyperspectral images.

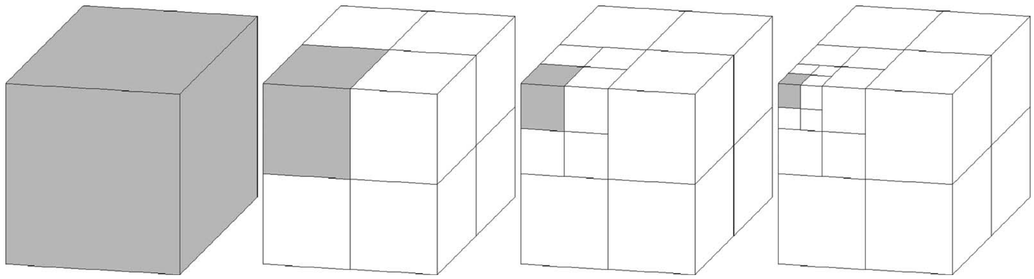

Figure 2. Graphical representation of the full 3D wavelet decomposition (three decomposition steps).

The used wavelet transform is a 3D extension of classical 2D wavelets. It produces a multidimensional wavelet transform by applying one level of decomposition to each dimension. Then iterate this procedure on the approximation cube until obtaining the suited number of decomposition levels (Figure 2).

Many works in literature have explored the 3D wavelet transform for multi/hyperspectral image compression but they only use isotropic 3D wavelets (same type of wavelets following all directions).[12,17,19–26] However, since the spectral dimension is generally lower than the spacial dimensions, it is appropriate to use a different type of wavelet filter for this dimension. Therefore we propose to use an anisotropic 3D wavelet transform that we realize with a CDF 9/7 filter following spatial dimensions and a Haar filter following spectral dimension. The choice of the spectral filter is built on the results obtained by Mansouri et al.[27] Indeed the authors have proposed the Haar lifting scheme wavelet basis as an appropriate short support basis for reflectance representation and estimation from multispectral images. This result met the conclusion of Kaarna and Parkkinen[28] where they recommend a short wavelet basis as a good choice for spectral wavelets.

Multi-2D Strategy

This strategy consists in applying the same 2D wavelet transform to each PCA eigenimages and finally a 2D SPIHT.[12,13,19] Because of PCA, the resulting image has decreasing energy bands, in order to take this fact into account, it is preferable to weight each band before applying SPIHT. As weight, we define the energy E of each band as in the formula

$$E = \frac{\sqrt{\sum_{x,y} I_{\lambda}(x,y)^2}}{XY}, \tag{1}$$

where I_{λ} is the image band centered at the λ wavelength, X and Y are its dimensions, and x and y are the positions of a pixel in the band.

Afterwards, we apply a 2D SPIHT coding to each band of the wavelet transform results to achieve compression.

Hybrid Strategy

The hybrid strategy (H3D) strategy consists in applying a hybrid rectangular/square 3D wavelet (Figure 3) to the PCA eigenimages cube as used in Ref. 25. The wavelets decomposition is composed by spatial CDF 9/7 filters and a spectral Haar filter. The fact that this wavelet transform has two differentiated stages (spatial transform is followed by spectral transform) allows its result to be considered as multiple 2D plans. For this reason we can apply 2D SPIHT coding to each resulting band to achieve compression, as in the M2D

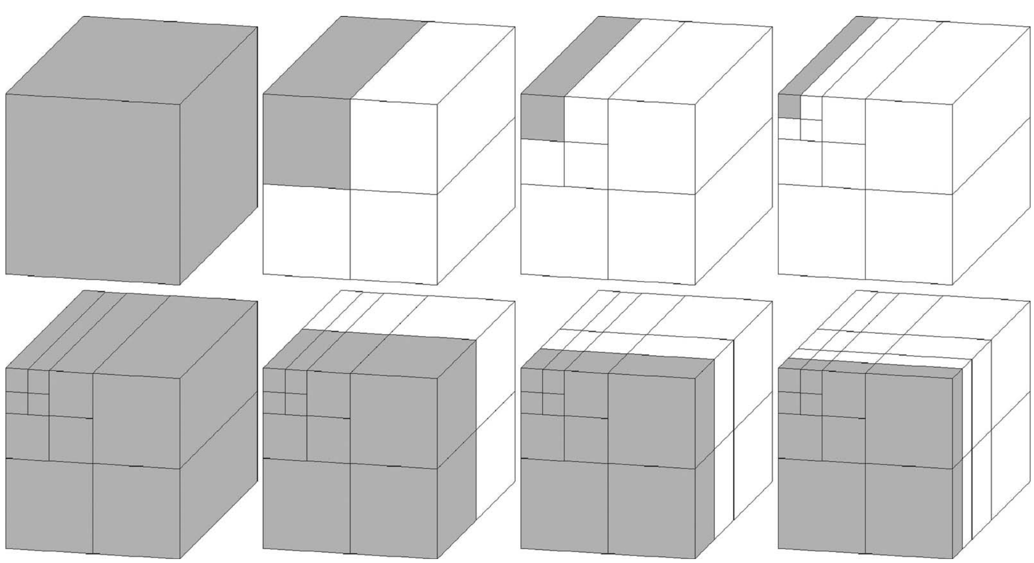

Figure 3. Graphical representation of the hybrid square/rectangular 3D wavelet decomposition (three decomposition steps). Spatial decompositions (top) followed by spectral decompositions (bottom).

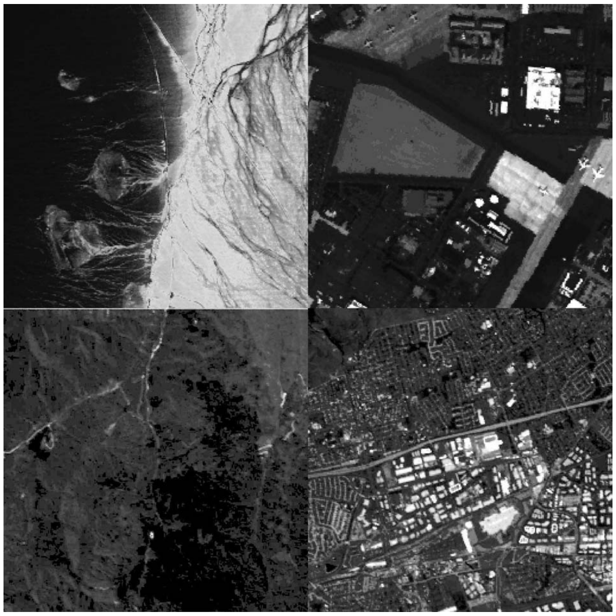

Figure 4. Multi/hyperspectral Aviris images we used in our experiments. Cuprite image (top left), SanDiego image (top right), JasperRidge (bottom left) and MoffettField (bottom right).

strategy (Fig. 1). In order to take the difference of energy bands into account, we weight each band with its energy E as in Eq. (1).

COMPRESSION EVALUATION FRAMEWORK

When lossy compression methods are used, quality measurements are necessary to evaluate performance. According to Eskicioglu,[29] the main problem in evaluating lossy compression techniques is the difficulty of describing the nature and importance of the degradations on the reconstructed image. Furthermore, in the case of ordinary 2D images, a metric has often has to reflect the visual perception of a human observer. This is not the case for hyperspectral images, which are first used through classification or detection algorithms. Therefore, metrics must correspond to applications. This is why instead of evaluating compression performances according to one metric or one type of metric, as in Ref. 30 where only one family of metrics is used [MSE, root mean square error (RMSE), and PSNR], we propose the use of nine known metrics belonging to four categories to evaluate performance. We call this a framework for compression evaluation.

The metrics we propose can be divided into four categories: signal processing isotropic extended metrics [PSNR, relative RMSE (RRMSE), mean absolute error (MAE), and maximum absolute distortion (MAD)], spectral oriented metrics [spectral fidelity (F_λ), maximum spectral angle (MSA), and goodness of fit coefficient (GFC)], an advanced statistical metric taking some perceptive aspects into account universal image quality index (UIQI), and a classification-oriented metric (K-means). Christophe et al.[31] show that the use of a set of metrics is more relevant than using just one. The PSNR is used in order to facilitate comparison with other methods since it is the metric most employed in image compression.

In the following sections this notation will be used: I is the original multispectral image and $\tilde{I}$ is the reconstructed multispectral image. The multispectral images are represented in three-dimensional matrix form: $I(x,y,\lambda)$, x is the pixel position in a row, y is the number of the row, and λ is the spectral band. n_x, n_y, and n_λ, respectively, the number of pixels in a row, the number of rows, and the number of spectral bands.

We also introduce the notation $I(x,y,\cdot)$ which stands for $I(x,y,\cdot)=\{I(x,y,\lambda)\,|\,1\leq\lambda\leq n_\lambda\}$. In this case $I(x,y,\cdot)$ corresponds to a vector of n_λ components.

For simplification, we note $I(x,y,\lambda)$ and $\tilde{I}(x,y,\lambda)$ by I and $\tilde{I}$, and also $\Sigma_{x=1}^{n_x}\Sigma_{y=1}^{n_y}\Sigma_{\lambda=1}^{n_\lambda}I$ by $\Sigma_{x,y,\lambda}I$.

Signal Processing Isotropic Extended Metrics

These metrics come from classic statistical measures. They do not take into account the difference between spatial and spectral dimensions. The structural aspect of errors does not appear.

Relative Root Mean Square Error

It is a classic statistical measure based on MSE (L_p norm) with a normalization by the signal level

$$\mathrm{RRMSE}(I,\tilde{I}) = \sqrt{\frac{1}{n_x n_y n_\lambda}\sum_{x,y,\lambda}\left(\frac{I-\tilde{I}}{I}\right)^2}. \tag{2}$$

Mean Absolute Error

$$\mathrm{MAE}(I,\tilde{I}) = \frac{1}{n_x n_y n_\lambda}\sum_{x,y,\lambda}|I-\tilde{I}|. \tag{3}$$

Maximum Absolute Distortion

The MAD is used to give a upper bound on the entire image.

$$\mathrm{MAD}(I,\tilde{I}) = \max\{|I-\tilde{I}|\}. \tag{4}$$

Spectral Oriented Metrics

These metrics are specially adapted for the multi/hyperspectral field.

Goodness of Fit Coefficient

The GFC is used here to evaluate the reconstruction of each reflectance spectrum

$$\mathrm{GFC}(I,\tilde{I}) = \frac{\left|\sum_j R_I(\lambda_j)R_{\tilde{I}}(\lambda_j)\right|}{\left|\sum_j [R_I(\lambda_j)]^2\right|^{1/2}\left|\sum_j [R_{\tilde{I}}(\lambda_j)]^2\right|^{1/2}}, \tag{5}$$

where $R_I(\lambda_j)$ is the original spectrum at wavelength λ_j and $R_{\tilde{I}}(\lambda_j)$ is the reconstructed spectrum at the wavelength λ_j.

The GFC is bounded, facilitating its understanding. We have $0\leq\mathrm{GFC}\leq 1$. The reconstruction is very good for $\mathrm{GFC}>0.999$ and perfect for a $\mathrm{GFC}>0.9999$.

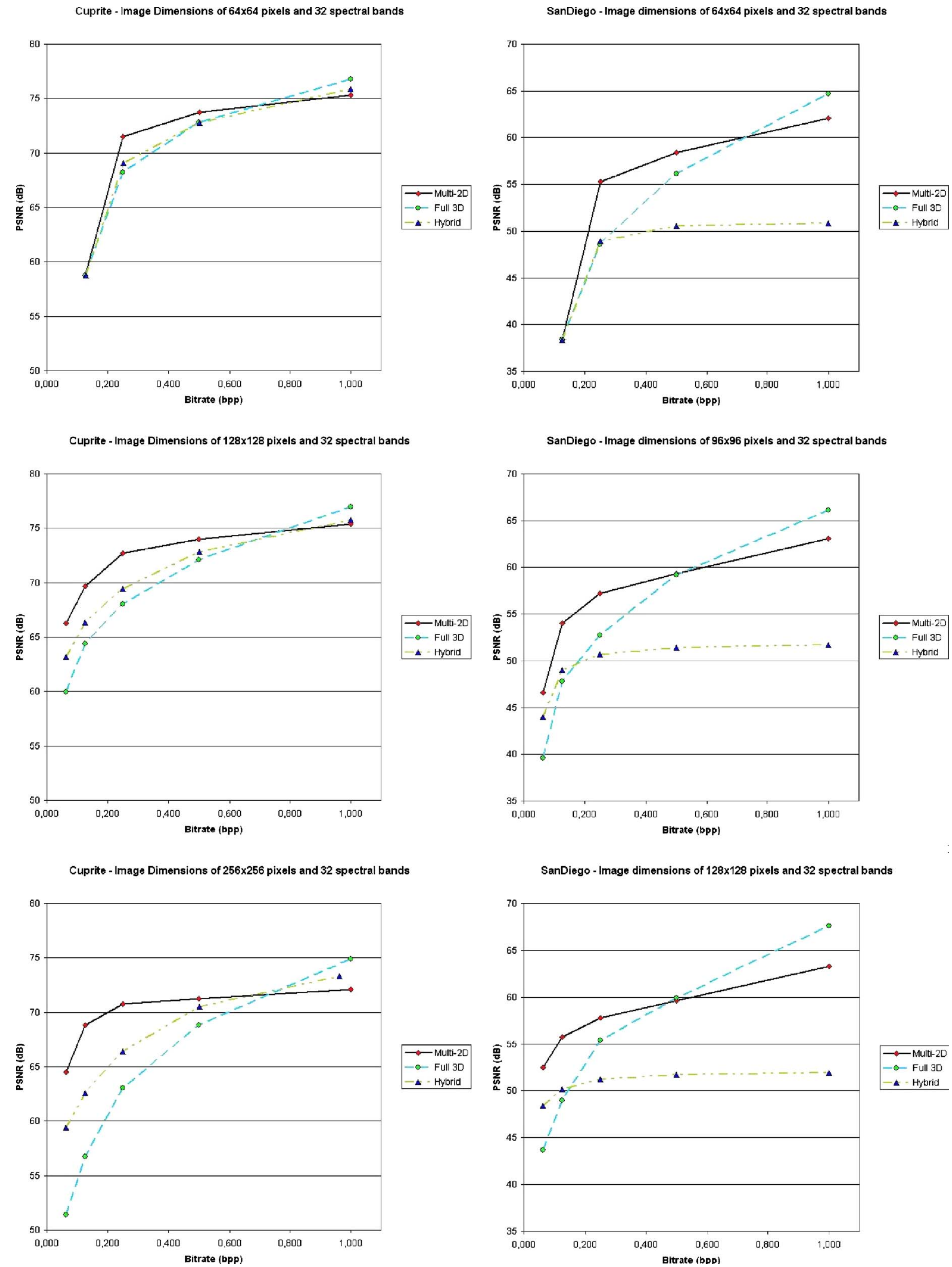

Figure 5. Compression results in terms of PSNR for 32 bands of the Cuprite image (left) with sizes of 64×64, 128×128 and 256×256 pixels and SanDiego image (right) with sizes of 64×64, 96×96 and 128×128 pixels.

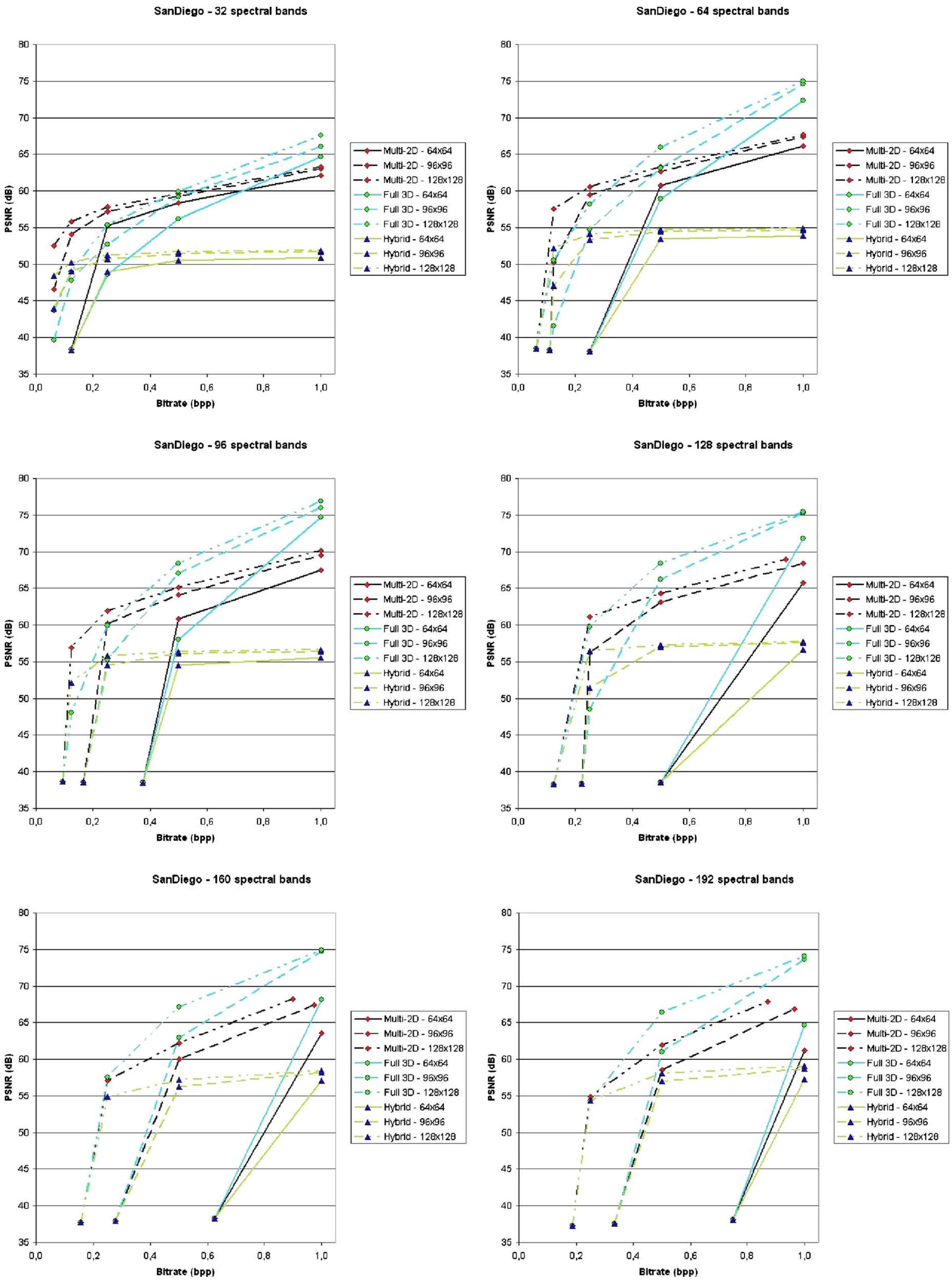

Figure 6. Compression results in terms of PSNR for 32, 64, 96, 128, 160 and 192 bands (SanDiego image).

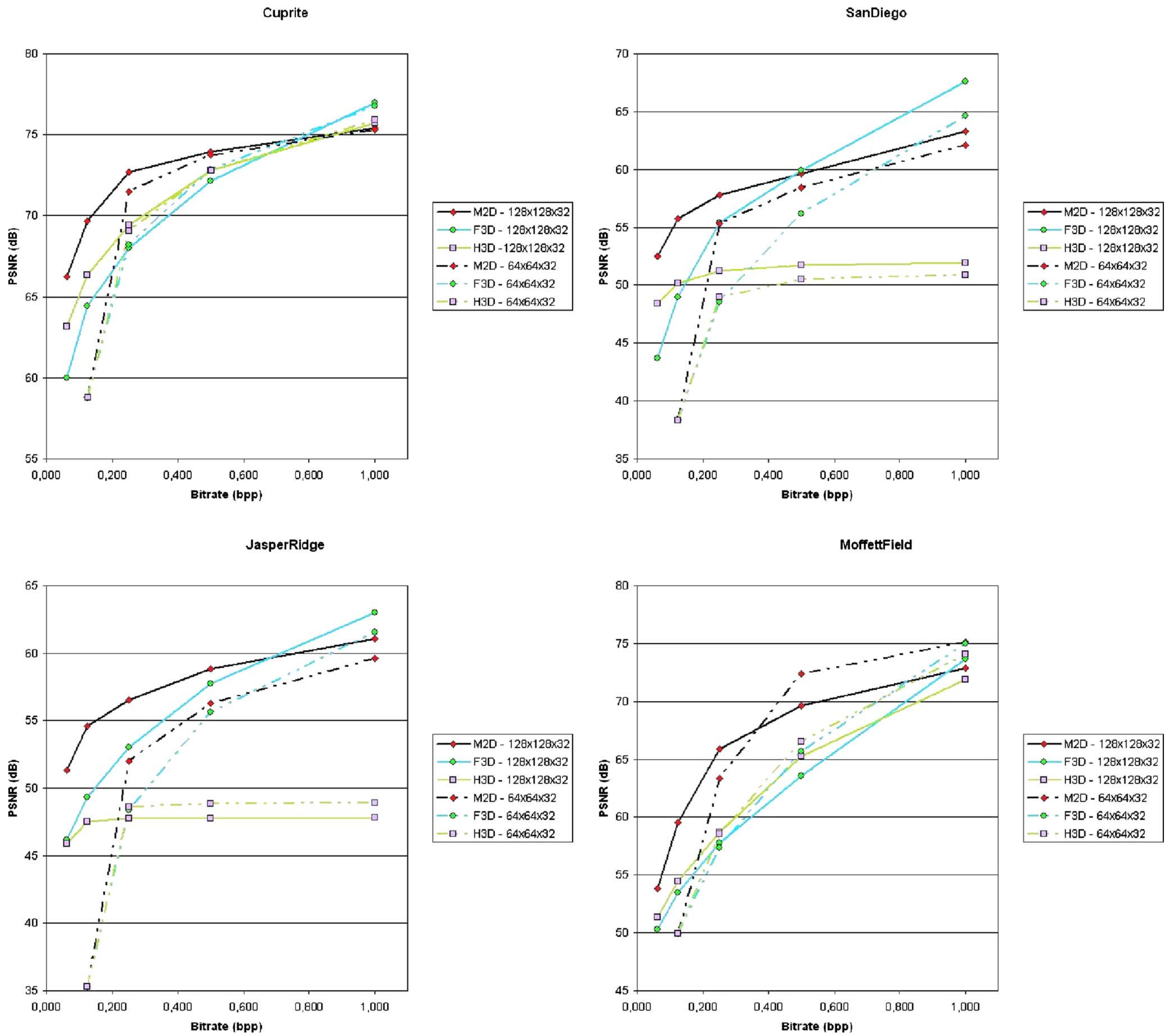

Figure 7. Compression results for Cuprite, SanDiego, JasperRidge and MoffettField images in terms of PSNR.

Spectral Fidelity (F_λ)
This metric was developed by Eskicioglu.[32] We define fidelity by

$$F(I,\tilde{I}) = 1 - \frac{\sum_{x,y,\lambda} [I-\tilde{I}]^2}{\sum_{x,y,\lambda} [I]^2}. \tag{6}$$

We will take into account the following adaptation focus on spectral dimension to obtain spectral fidelity

$$F_\lambda(I,\tilde{I}) = \min_{x,y}\{F(I(x,y,\cdot),\tilde{I}(x,y,\cdot))\}. \tag{7}$$

Maximum Spectral Angle
The MSA is a metric used in Ref. 33 The spectral angle represents the angle between two spectra viewed as vectors in an n_λ-dimensional space

$$\mathrm{SA}_{x,y} = \cos^{-1}\left(\frac{\sum_\lambda I\cdot\tilde{I}}{\sqrt{\sum_\lambda I^2 \sum_\lambda \tilde{I}^2}}\right). \tag{8}$$

In our case we take the maximum of SA with:

$$\mathrm{MSA} = \max_{x,y}(\mathrm{SA}_{x,y}). \tag{9}$$

Universal Image Quality Index
The UIQI was developed by Wang[34] for monochrome images. This metric uses structural distortion rather than error sensibility. It is an advanced statistical metric. The UIQI is based on three factors: loss of correlation, luminance distortion, and contrast distortion;

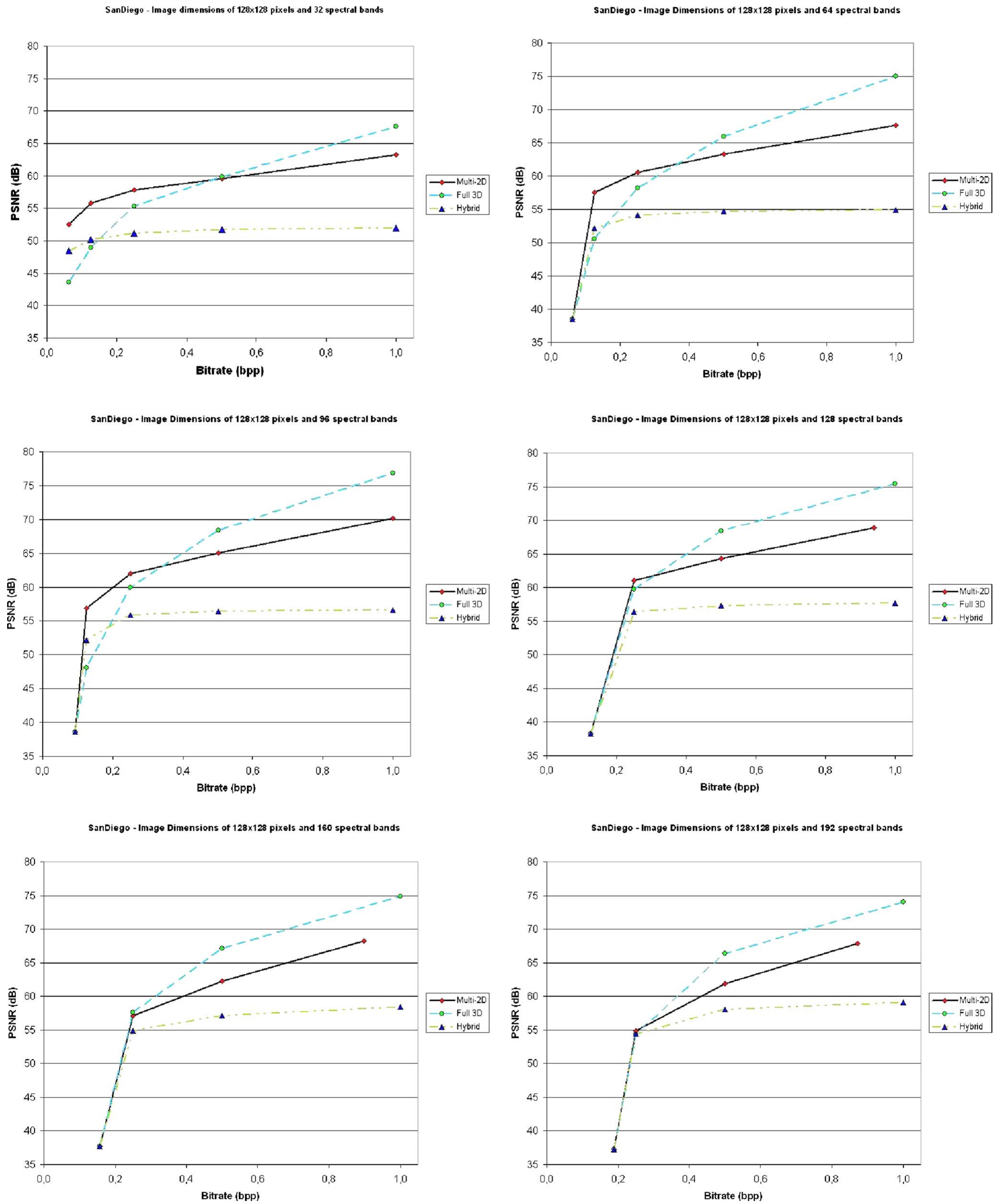

Figure 8. Compression results in terms of PSNR for 128 × 128 spatial dimensions (SanDiego image).

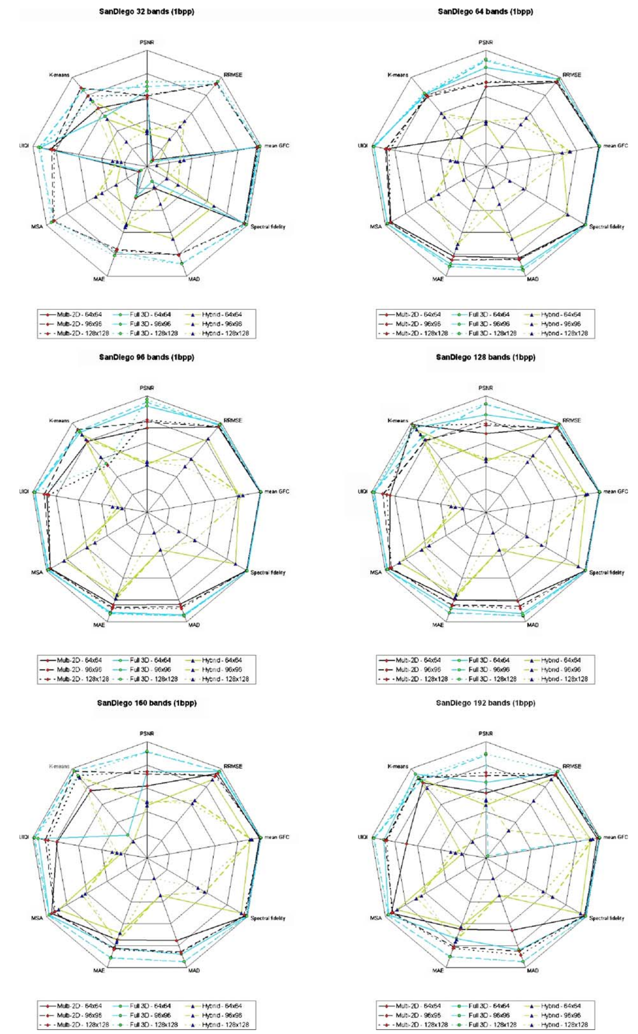

Figure 9. Compression results for 32, 64, 96, 128, 160 and 192 bands of the SanDiego image with a bitrate of 1 bpp.

$$Q(U,V) = \frac{4\sigma_{UV}\mu_U\mu_V}{(\sigma_U^2+\sigma_V^2)(\mu_U^2+\mu_V^2)}, \tag{10}$$

where σ_{UV} is the cross correlation $E[(U-\mu_U)(V-\mu_V)]$, μ is the mean, and σ^2 is the variance. The result is bounded by $-1 \leq Q \leq 1$.

The UIQI can be applied in three different ways, on each band, on each spectrum of the image or on both. We use it on each spectral band of the image as follows:

$$Q_{x,y} = \min_{\lambda}\{Q(I(\cdot,\cdot,\lambda),\tilde{I}(\cdot,\cdot,\lambda))\}. \tag{11}$$

Classification Driven Metric

As a classification method we use the K-means, and as metric we compute the percentage of misclassified pixels for the compressed images compared to the noncompressed image.

The K-means method is a well-known geometric clustering algorithm based on work by Lloyd in Ref. 35. Given a set of n data points, the algorithm uses a local search approach to partition the points into k clusters. Let X a set of k initial cluster centers is chosen arbitrarily. Each point is then assigned to the center closest to it, and the centers are recomputed as centers of mass of their assigned points. This is repeated until the process stabilizes. It can be shown that no partition occurs twice during the course of the algorithm, and so the algorithm is guaranteed to terminate.

Let $X=\{x_1,x_2,\ldots,x_n\}$ be a set of points in $\mathsf{R}d$. After being seeded with a set of k centers $c_1,c_2,\ldots,c_k$ in $\mathsf{R}d$, the algorithm partitions these points into clusters as follows:

1. For each $i \in \{1,\ldots,k\}$, set the cluster C_i to be the set of points in X that are closer to C_i than they are to C_j for all $j \neq i$.
2. For each $i \in \{1,\ldots,k\}$, set c_i to be the center of mass of all points in C_i: $c_i = 1/|C_i| \Sigma_{x_j \in C_i} x_j$.
3. Repeat steps 1 and 2 until c_i and C_i no longer change, at which point return the cluster C_i.

If there are two centers equally close to a point in X, we break the tie arbitrarily. If a cluster has no data points at the end of step 2, we eliminate the cluster and continue as before. Our lower bound construction will not rely on either of these degeneracies.

EXPERIMENTS AND RESULTS

We conducted our experiments on the largely used AVIRIS (http://aviris.jpl.nasa.gov) images (Cuprite, SanDiego, JasperRidge, and MoffettField). These images represent very different landscapes, Cuprite and JasperRidge represent uniform spatial areas whereas SanDiego represents an airport and MoffettFiel represents an urban landscape with many high frequencies (Figure 4).

Experiments

First Experiment

The first experiment we conducted aimed to compare the performance of the F3D strategy with M2D and H3D strategies regarding different compression bitrates when using different spatial dimensions of images. We conducted the experiments on 32 bands of the Cuprite image with spatial dimensions of 64×64, 128×128, and 256×256 pixels, on 32 bands of the SanDiego image with spatial dimensions of 64×64, 96×96, and 128×128 pixels, on 32 bands of the JasperRidge and MoffettField images with spatial dimensions of 64×64 and 128×128 pixels. All images are coded in 16 bit integer.

Second Experiment

The second experiment sought to evaluate the performance of the F3D strategy with M2D and H3D strategies regarding to different compression bitrates when the number of bands changes. So we used different spatial sizes of the SanDiego multi/hyperspectral image with different number of bands (32, 64, 96, 128, 160, and 192).

Third Experiment

The third experiment concerns compression by tile. It is interesting to cut large images into sets of smaller ones to reduce compression memory needs and also to parallelize compression computation to reduce computation time. We

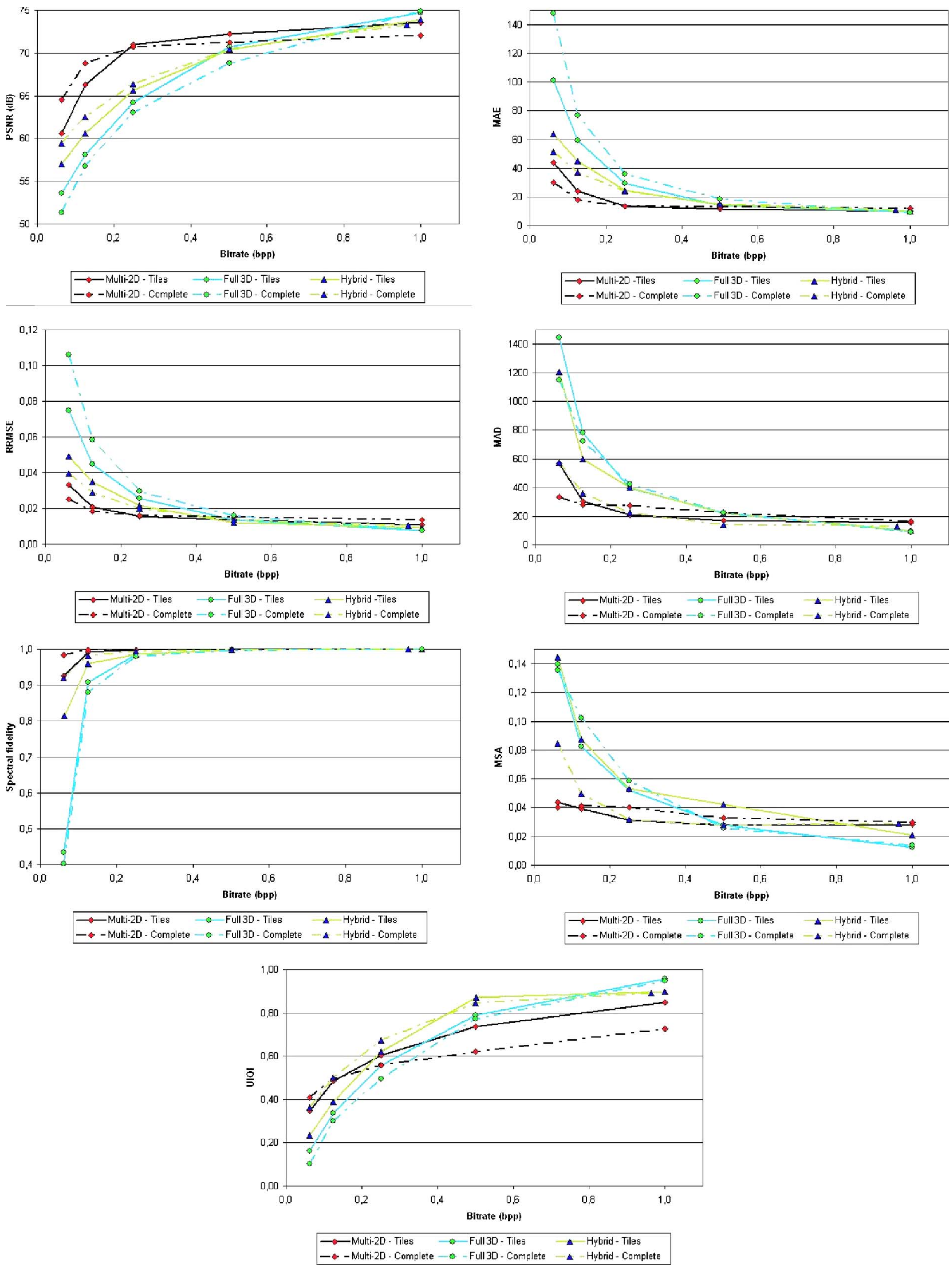

Figure 10. Comparison between tiles compression results and complete image compression results for 32 bands of the Cuprite image.

Table I. Results in terms of statistics on GFC; on the top: tile compression results, on the bottom: compression result of the complete image.

			M2D		
Bitrate	0.0625	0.1250	0.2500	0.5000	1.0000
Mean GFC	0.9999	1.0000	1.0000	1.0000	1.0000
Std GFC	0.0000	0.0000	0.0000	0.0000	0.0000
Max GFC	1.0000	1.0000	1.0000	1.0000	1.0000
Min GFC	0.9990	**0.9992**	**0.9995**	**0.9996**	**0.9996**
Median GFC	1.0000	1.0000	1.0000	1.0000	1.0000
Mean GFC	0.9999	0.9999	1.0000	1.0000	1.0000
Std GFC	0.0000	0.0001	0.0001	0.0000	0.0000
Max GFC	1.0000	1.0000	1.0000	1.0000	1.0000
Min GFC	**0.9892**	**0.9992**	0.9992	0.9995	**0.9996**
Median GFC	1.0000	1.0000	1.0000	1.0000	1.0000
			F3D		
Bitrate	0.0625	0.1250	0.2500	0.5000	1.0000
Mean GFC	0.9998	0.9999	0.9999	1.0000	1.0000
Std GFC	0.0004	0.0001	0.0001	0.0000	0.0000
Max GFC	1.0000	1.0000	1.0000	1.0000	1.0000
Min GFC	0.9902	**0.9966**	**0.9986**	0.9996	**0.9999**
Median GFC	0.9999	0.9999	1.0000	1.0000	1.0000
Mean GFC	0.9994	0.9998	0.9999	1.0000	1.0000
Std GFC	0.0005	0.0002	0.0001	0.0000	0.0000
Max GFC	1.0000	1.0000	1.0000	1.0000	1.0000
Min GFC	**0.9908**	0.9948	0.9983	**0.9997**	**0.9999**
Median GFC	0.9996	0.9999	0.9999	1.0000	1.0000
			H3D		
Bitrate	0.0625	0.1250	0.2500	0.5000	1.0000
Mean GFC	0.9999	0.9999	0.9999	1.0000	1.0000
Std GFC	0.0004	0.0001	0.0001	0.0000	0.0000
Max GFC	1.0000	1.0000	1.0000	1.0000	1.0000
Min GFC	0.9896	0.9962	0.9986	0.9991	**0.9998**
Median GFC	0.9999	0.9999	1.0000	1.0000	1.0000
Mean GFC	0.9999	0.9999	1.0000	1.0000	1.0000
Std GFC	0.0001	0.0001	0.0000	0.0000	0.0000
Max GFC	1.0000	1.0000	1.0000	1.0000	1.0000
Min GFC	**0.9964**	**0.9988**	**0.9995**	**0.9996**	0.9996
Median GFC	0.9999	1.0000	1.0000	1.0000	1.0000

conducted the experiment on the Cuprite AVIRIS image with a size of 256×256 pixels and 32 bands. We cut this image into four tiles of 128×128 pixels and compressed each tile with the F3D, M2D, and H3D strategies. We then reconstructed the original image with the four tiles, apply metrics to it, and compared results with complete image metric results. Results in terms of PSNR, MAE, RRMSE, MAD, F_{λ}, MSA, and UIQI are shown in Figure 10, and in terms of GFC in Table I.

Results

Representing the results of the experiments within the framework of nine metrics is difficult. A good way to represent the results is to use a star (radar) diagram (as in Ref. 36) which gives a more compact and intuitive vision than a classical x-y representation in this case. The nine axes of the diagram correspond to the nine metrics. All star diagrams have the same scale, minimum and maximum are given on each axis for graphical interpretation and ease of compari-

Table II. Compression result in terms of percentage of misclassified pixels using K-means classifier for the SanDiego image at a bitrate of 1 bpp.

64*64 spatial image size						
Strategies	Number of bands					
	32	64	96	128	160	192
F3D	8.76%	**3.71%**	**2.10%**	0.98%	5.13%	**1.15%**
M2D	**6.86%**	13.45%	4.08%	**0.34%**	4.88%	3.20%
H3D	9.38%	13.38%	2.61%	1.51%	**3.71%**	2.15%
96*96 spatial image size						
Strategies	Number of bands					
	32	64	96	128	160	192
F3D	2.90%	**3.91%**	1.79%	**3.13%**	0.47%	2.68%
M2D	**2.30%**	4.35%	**1.50%**	3.83%	**0.44%**	**2.02%**
H3D	4.89%	8.00%	3.61%	3.71%	1.63%	16.41%
128*128 spatial image size						
Strategies	Number of bands					
	32	64	96	128	160	192
F3D	5.42%	**3.58%**	9.07%	**0.54%**	**1.53%**	2.03%
M2D	**4.16%**	4.01%	9.44%	0.73%	1.58%	**1.92%**
H3D	14.49%	8.90%	**7.61%**	2.50%	1.93%	4.32%

son. Axes of RRMSE, MAD, MAE, MSA, and K-means are inverted, the extremity corresponds to minimum degradation and the origin of the axes corresponds to maximum degradation. This representation permits good readability but does not allow us to show bitrate variation. Which is why in Figure 9 we only show results for a bitrate of 1 bpp.

When necessary, we highlight some results by giving some tables and diagrams related to the particular metrics. We often represent results in terms of PSNR in order to facilitate comparison with other studies since it is the metric most employed in image compression.

First Experiment Results

The results of the first experiment (regarding image spatial dimension variations) in term of PSNR are represented in Figure 5 for the Cuprite image and in Figure 6 for the SanDiego image. Results show that the F3D strategy outperforms M2D and H3D strategies for high bitrate values especially for large image spatial dimensions. For small bitrate values M2D strategy gives the best results. The H3D strategy never has the best results.

Results presented in Figure 7 show that compression results for the four images used have the same trend. This trend is characterized by the fact that for small bitrate values, the M2D strategy gives the best results, and for high bitrate values it is the F3D strategy which gives the best results.

Second Experiment Results

For the second experiment on the SanDiego image, graphics in Figures 6 and 8 show that F3D strategy always outperforms the two other compression strategies for high bitrate values. When the number of spectral bands increases the F3D strategy outperforms the two other strategies for smaller bitrate values (for 160 and 192 spectral bands the F3D strategy give the better results for all bitrate values).

M2D and F3D strategies have the best score for 96 bands. When the number of bands deviates from this value of 96 bands, results decrease proportionally. For the H3D strategy PSNR results increase proportionally to the number of bands. PSNR and other metrics show the same trends.

Star diagrams for SanDiego images of 32, 34, 96, 128, 160, and 196 spectral bands with a bitrate of 1 bpp (Fig. 9) show that not all metrics have the same trend. This is particularly visible for the H3D strategy with PSNR, GFC, MAD, MAE, and UIQI which have similar results but RRMSE, F_λ and MSA have inverted results. For M2D and F3D strategies all results are similar except regarding to the UIQI metric.

We can also see in Table II that results in terms of percentage of misclassified pixels using K-means are the worst for H3D strategy. We notice that results regarding classification metric for M2D and F3D strategies are quite similar.

Third Experiment Results

Results of the tiling experiment shown in Fig. 10 and in Table I permit a comparison of tile compression with complete image compression. In terms of GFC, the most relevant values are for GFC minimum.

We can note for all metrics that the tile compression results are better than the complete image compression results for high bitrate values, but for small bitrate values it is

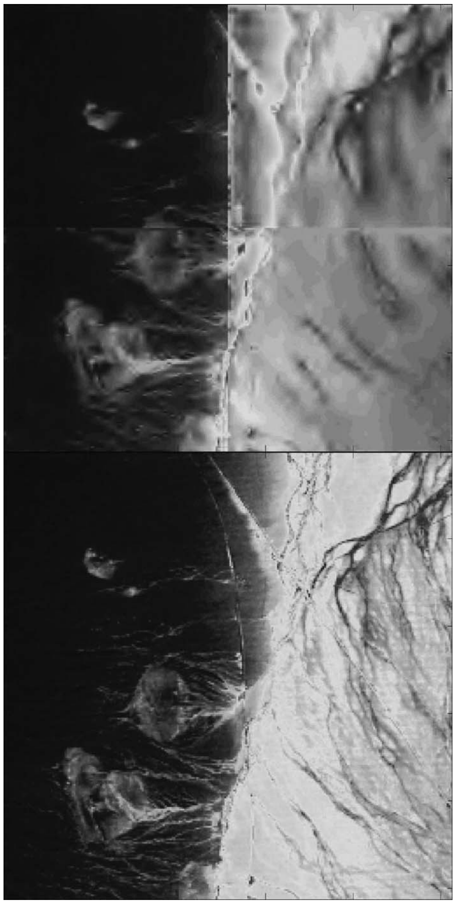

Figure 11. Tile hybrid compression result example. On the top: band nine of the Cuprite image at a bitrate of 0.0625 bpp; On the bottom: the same band at a bitrate of 0.5 bpp. For a bitrate of 0.0625 bpp we can remark creation of virtual edges between tiles and spatial smoothing. These two effects are not visible for a 0.5 bpp bitrate.

inverted, the inversion points are different depending on metrics. These results are due to sizeable spatial discontinuities for small bitrate values as shown in Figure 11, in which we depict an example of H3D compression at 0.0625 and 0.5 bpp bitrates.

DISCUSSION

The first two experiments we performed allow us to compare F3D strategy with M2D and H3D strategies following spatial and spectral dimensions variations. A general trend is observed: for high bitrate values, the F3D strategy gives the best results and for small values of bitrate the M2D strategy gives the best results. Results of the H3D strategy are between the two other strategies. This trend could be explained by two major points:

- For small values of bitrates the F3D strategy gives bad results because of that the 3D SPIHT used in this strategy uses lists (list of significant and insignificant pixels, list of insignificant sets) which grow up very fast compared to lists of 2D SPIHT (each pixel has eight children for the 3D version and only four in 2D). And for high values of bitrates fewer coefficients are added to the lists than for the 2D version. This could explain the fact that the M2D strategy gives better results than F3D strategy only for small values of bitrates.
- The H3D strategy gives bad results because it is a combination of 2D and 3D strategies. So using a 2D SPIHT after a 3D decomposition is not the optimal way.

The third experiment allows us to measure tiling effects. For all metrics the tile compression results are better than the complete image compression results for high bitrate values and it is inverted for small bitrate values. These results are mainly caused by spatial discontinuities between each tile which are strongly marked for small bitrate values (creation of virtual edges between tiles) and spatial smoothing. These two effects tend to fade when the compression bitrate growing.

We can estimate speed and memory need for each compression strategy by comparing it to the two others for each part of the compression.

First we applied spectral PCA for all strategies, taking the same amount of time and memory. Second we applied wavelet decompositions. For the F3D and H3D strategies, decompositions are very similar and are performed on the entire image; they take similar computation times and computation memory. For the M2D strategy it depends on the implementation of the algorithm. If we consider each band of the image separately, the decomposition of the entire image takes a little more time than 3D decompositions but less memory (a ratio equal to the number of bands). We can also apply all 2D decompositions to the image at the same time: the spectral wavelet decomposition time is less but requires as much memory as in 3D decompositions. Finally we applied SPIHT and 3D SPIHT algorithms. These algorithms are identical, the only differences are the number of pixels with children (three over four for SPIHT and seven over eight for 3D SPIHT), the number of children (four for SPIHT and eight for 3D SPIHT), and their positions. The 3D SPIHT is slower than SPIHT and also takes more memory.

The speed and memory used by the three algorithms depend on image complexity but also on algorithm implementations. The M2D strategy is the fastest, ahead of the H3D strategy; the F3D strategy is the slowest. The F3D strategy also requires more memory than the two other. For large spatial dimension images the tiling compression allows to parallelize computation but results show that it is better to use high bitrate values to limit degradations introduced by the compression.

CONCLUSION

In this article, we have proposed an anisotropic full 3D wavelets implementation for multi/hyperspectral images compression strategy (F3D), and compared it with two other strategies. These strategies are M2D and H3D compressions. All strategies are combined with a spectral PCA decorrelation for energy compaction. We also proposed a evaluation framework containing nine metrics belonging to four different families: signal processing isotropic extended metrics, spectral oriented metrics, perceptive metrics, and classification-oriented metrics. The comparison of these strategies within this framework show the same trend for most metrics: the F3D strategy is better than M2D and H3D strategies for high bitrate values. F3D strategy results are better for large spatial image dimensions and for a great number of spectral bands.

ACKNOWLEDGMENT

The authors wish to thank Carmela Chateau for proofreading the English.

REFERENCES

1 M. Boliek, C. Christopoulos, and E. Majani, JPEG 2000 Part I Final Committee Draft Version 1.0. *ISO/IEC JTC*, 1, (2000).

2 M. Boliek, E. Majani, J. S. Houchin, J. Kasner, and M. L. Carlander, "JPEG 2000 part II final committee draft: *ISO/IEC JTC1/SC29/WG1*", FCD, 15444, 2 (2000).

3 C. Christopoulos, A. Skodras, and T. Ebrahimi, "The JPEG 2000 still image coding system: An overview", IEEE Trans. Consum. Electron. **46**, 1103–1127 (2000).

4 D. S. Taubman, "High Performance Scalable Image Compresssion with EBCOT", IEEE Trans. Image Process. **9**(7), 1158 (2000).

5 D. S. Taubman and M. W. Marcellin, "JPEG 2000 Image Compression Fundamentals, Standards and Practice," Kluwer International Series in Engineering and Computer Science, SECS 642 (2002).

6 S. Gupta and A. Gersho, "Feature predictive vector quantization of multispectral images", IEEE Trans. Geosci. Remote Sens. **30**, 491–501 (1992).

7 G. P. Abousleman, M. W. Marcellin, and B. R. Hunt, "Compression of hyperspectral imagery using the 3D DCT and hybrid DPCM/DCT", IEEE Trans. Geosci. Remote Sens. **33**, 26–34 (1995).

8 J. A. Saghri and A. G. Tescher, "Near-lossless bandwidth compression for radiometric data (Journal Paper)", Opt. Eng. **30**, 934–939 (1991).

9 P. Ready and P. Wintz, "Information extraction, SNR improvement, and data compression in multispectral imagery", *Communications, IEEE Transactions on [legacy, pre-1988]*, **21**(10), 1123–1131 (1973).

10 B. Epstein, R. Hingorani, J. Shapiro, and M. Czigler, "Multispectral image compression by wavelet/Karhunen-Loeve transformation", IGARSS **92**, 672–674 (1992).

11 J.-C. Harsanyi and C.-I. Chang, "Hyperspectral image classification and dimensionality reduction: An orthogonal subspace projection strategy", IEEE Trans. Geosci. Remote Sens. **32**, 779–785 (1994).

12 J. Mielikäinen and A. Kaarna, "Improved back end for integer PCA and wavelet transforms for lossless compression of multispectral images", *Proc. 16th International Conference on Pattern Recognition* (IEEE Computer Society, Quebec, Canada, 2002), Vol. **2**, pp. 257–260.

13 Q. Du and J. E. Fowler, "Hyperspectral image compression using JPEG2000 and principal component analysis", IEEE Geosci. Remote Sens. Lett. **4**, 201–205 (2007).

14 L. Chang, C. M. Cheng, and T. C. Chen, "An efficient adaptive KLT for multispectral image compression", *Proc. 4th IEEE Southwest Symp. Image Anal. and Interpretation* (IEEE, Piscataway, NJ, 2000) pp. 252–255.

15 Y. Gu, Y. Zhang, and J. Zhang, "A kernel based nonlinear subspace projection method for reduction of hyperspectral image dimensionality", *Proc. 2002 International Conference on Image Processing* (IEEE, Rochester, NY, 2002) pp. 357–360.

16 A. Said and W. A. Pearlman, "A new, fast, and efficient image codec based on set partitioning in hierarchical trees", IEEE Trans. Circuits Syst. Video Technol. **6**, 243–250 (1996).

17 B.-J. Kim and W. A. Pearlman, "An embedded wavelet video coder using three-dimensional set partitioning in hierarchical trees (SPIHT)", *Proc. Data Compression Conference, 1997* (IEEE, Snowbird, UT, 1997) pp. 251–260.

18 L. Dragotti, G. Poggi, and A. R. P. Ragozini, "Compression of multispectral images by three-dimensional SPIHT algorithm", IEEE Trans. Geosci. Remote Sens. **38**, 416–428 (2000).

19 A. Kaarna, P. Toivanen, and P. Keränen, "Compression and classification methods for hyperspectral images", Pattern Recognition and Image Analysis **16**, 413–424 (2006).

20 A. Kaarna, P. Zemcik, H. Kaelviainen, and J. Parkkinen, "Multispectral image compression", *Proc. International Conference On Pattern Recognition* (IEEE Computer Society Press, Los Alamitos, CA, 1998) pp. 1264–1267.

21 A. Kaarna and J. Parkkinen, "Wavelet filter selection in multispectral image compression", *Proc. International Conference On Pattern Recognition* (IEEE Computer Society Press, Los Alamitos, CA, 2000) pp. 242–245.

22 A. Kaarna and J. Parkkinen, "Comparison of compression methods for multispectral images", *Proc. NORSIG-Nordic Signal Processing Symposium* (IEEE, Kolmarden, Sweden, 2000) pp. 251–254.

23 A. Kaarna, "Integer PCA and wavelet transforms for multipectral image compression", *Proc. International Geoscience and Remote Sensing Symposium, IEEE IGARSS'2001* (IEEE, Piscataway, NJ, 2001) pp. 1853–1855.

24 S. Lim, K. H. Sohn, and C. Lee, "Compression for hyperspectral images using three dimensional wavelet transform", *Proc. International Geoscience and Remote Sensing Symposium, IEEE IGARSS'2001* (IEEE, Piscataway, NJ, 2001) pp. 109–111.

25 B. Penna, T. Tillo, E. Magli, and G. Olmo, "Progressive 3D coding of hyperspectral images based on JPEG 2000", IEEE Geosci. Remote Sens. Lett. **3**, 125–129 (2006).

26 X. Tang, S. Cho, and W. A. Pearlman, "3D set partitioning coding methods in hyperspectral image compression", *Proc. IEEE International Conference on Image Processing (ICIP'03)* (IEEE, Piscataway, NJ, 2003) pp. 239–242.

27 A. Mansouri, T. Sliwa, J. Y. Hardeberg, and Y. Voisin, "Representation and estimation of spectral reflectances using projection on PCA and wavelet bases", Color Res. Appl. **33**, 485–493 (2008).

28 A. Kaarna and J. Parkkinen, "Wavelet compression of multispectral images", *Proc. IASTED International Conference on Computer Graphics and Imaging* (ACTA-Press, Halifax, Canada, 1998) pp. 142–145.

29 A. M. Eskicioglu and P. S. Fisher, "Image quality measures and their performance", IEEE Trans. Commun. **43**, 2959–2965 (1995).

30 B. Shrestha, C. G. O'Hara, and N. H. Younan, *JPEG2000: Image Quality Metrics* (American Society for Photogrammetry and Remote Sensing, Baltimore, MD, 2005).

31 E. Christophe, D. Léger, and C. Mailhes, "Quality criteria benchmark for hyperspectral imagery", IEEE Trans. Geosci. Remote Sens. **43**, 2103 (2005).

32 A. M. Eskicioglu and P. S. Fisher, "A survey of quality measures for gray scale image compression", *AIAA 9th Computing in Aerospace Conference* (AIAA, San Diego, CA, 1993) pp. 304–313.

33 N. Keshava and J. F. Mustard, "Spectral unmixing", IEEE Signal Process. Mag. **19**, 44–57 (2002).

34 Z. Wang and A. C. Bovik, "A universal image quality index", IEEE Signal Process. Lett. **9**(3), 81 (2002).

35 S. P. Lloyd, "Least squares quantization in PCM", IEEE Trans. Inf. Theory **28**, 129–137 (1982).

36 E. Christophe, D. Léger, and C. Mailhes, "New quality representation for hyperspectral images". *Proc. International Society for Photogrammetry and Remote Sensing* (ISPRS, Beijing, China, 2008) pp. 315–320.